Arabian Journal of Geosciences (2022) 15: 1010
https://doi.org/10.1007/s12517-022-10242-y

ORIGINAL PAPER

Dynamics of land surface temperature (LST) and their relation with urban biophysical components in Gorakhpur (India) urban area: a GIS and statistical based analysis for sustainable planning

Nutan Tyagi[1] · **Santanu Sahoo**[2]

Received: 27 July 2021 / Accepted: 28 April 2022 / Published online: 18 May 2022

Abstract
Expansion of built-up area in and around urban areas has resulted in an increase in air and land surface temperature of cities, thus resulting in the creation of urban heat islands. Rapid growth of Gorakhpur urban area has experienced land use transformation, and this has resulted in increased built-up area which has consequently affected the surface temperature of the area. The identification of these areas provides better understanding of urban landscape. The study aims to investigate the land use/land cover transformation, status of impervious surface, land surface temperature, and its association with biophysical parameters such as normalized difference vegetation index, normalized difference built-up index, normalized difference water index, modified normalized difference water index, normalized difference bareness index, bare soil index, soil-adjusted vegetation index, and land surface temperature for Gorakhpur urban area. Multiple linear regression analysis has been used to find out the variables, which are affecting the land surface temperature the most. The land surface temperature of the area has been assessed using thermal band (6th) of the Landsat Thematic Mapper 5 (TM) satellite images for four time periods of 1990, 2000, 2010, and 2019. Getis-Ord Gi* statistics has been applied to analyze the clustering and spatio-temporal dynamics of hot spots of land surface temperature. Analysis of land use/land cover revealed that the highest changes (23.77%) among land use classes occurred in built-up area and the highest decline (−20.90%) is observed in agricultural land use class during 1990 to 2019. As a result, there is an increase in impervious surface and also in mean land surface temperature, which was 18.33 °C in 1999 and increased to 20.52 °C in 2019. Thus, overall 2.3 °C temperature has increased during the study period. The correlation coefficient between land surface temperature and biophysical parameter shows continuous increasing high positive relationship between the bare soil index and the normalized difference built-up index.

Keywords Land use/land cover (LU/LC) · Accuracy assessment · Land surface temperature (LST) · Biophysical indices · Multiple linear regression · Hot spot · Gorakhpur urban area (GUA)

Introduction

Rapid urbanization in the world is quite alarming, especially in developing countries such as India (Kumar et al. 2007). Horizontal expansion of urban areas is continuously increasing and is consuming agricultural area of its periphery, thereby increasing input impervious surface through expansion and densification of these urban areas. Land cover alteration is replacing natural surfaces with man-made surfaces. Transformation of land use has *promoted* many meteorological problems like urban heat island and change in the climate at micro-level everywhere in the world (Ridd 1995). Population pressure, reduction in green areas, increase in impervious surfaces through land use transformation in various urban activities, and heavy traffic load have

Responsible Editor: Amjad Kallel

✉ Nutan Tyagi
nutan_tyagi@yahoo.com

Santanu Sahoo
sahoosantanuraj@gmail.com

[1] School of Humanities and Social Sciences (SHSS), Sharda University, Greater Noida, UP, India

[2] Department of Geography, D.D.U. Gorakhpur University, Gorakhpur, UP, India

further added thermal stress on the city and changed the thermal character of the areas, making them warmer than the surroundings, which has a negative impact on the urban ecosystem and nearby region. Urban heat island is the result of this process. This phenomenon is present in almost all the big and small cities but of course with varying intensity and magnitude around the world. In developing countries, unplanned growth of the cities and reduction of greeneries are aggravating and complicating this problem. Million cities of India are expanding at a much faster rate than the rest, and almost all are facing the same problem coupled with other environmental problems. India's urban population by 2036 is expected to reach 594 million, which was 377 million in 2011. As per 2011 census of India, 31% population of the country is living in urban areas, which is expected to rise up to 60% by 2050 (https://censusindia.gov.in/2011census/population_enumeration.html/).

The estimation of land surface temperature (LST) is essential to know the pattern of temporal changes in the temperature and also to identify those areas, which need immediate attention and require mitigation measures. Many studies have been carried out to study the variability between greenness and surface temperature and tried to assess the present status of land surface temperature (Weng et al. 2004, Raynolds et al. 2008; Mallick et al. 2008; Sheik 2019) and also suggested measures to cope up with this problem.

Land surface temperature (LST) is an important factor for the determination of several biophysical parameters and processes. Remote sensing images provide very useful information for extraction, determination, and measurements of land surface temperature (LST). It enables to monitor surface energy influx, evapotranspiration, crop production, near surface temperature etc. and also its association with the land use (Owen et al. 1998; Stisen et al. 2007; Xiao et al. 2008; Li et al. 2009; Amiri et al. 2009; Jiang and Tian 2010; Dontree 2010; Liu et al. 2017, and Igun and Williams 2018; Liu et al. 2020; Imran et al. 2021).

The results of various studies clearly conclude that there is a strong relationship between the LST (land surface temperature) and land use/land cover class. Availability of remote sensing data has opened up a new dimension in the study of land surface temperature (LST)/UHI. A wide range of sensors, like Landsat 4 and 5 (TM), 7 (ETM+), 8 (TIRS 1 and 2), Advanced Spaceborne Thermal Emission and Reflection (ASTER), Moderate Resolution Imaging Spectroradiometer (MODIS), Advanced Very High-Resolution Radiometer (AVHRR), and others are utilized for the extraction of land surface temperature (LST). Many scholars have studied heat islands and land surface temperature and have suggested mitigation measures.

Generally, biophysical components are defined as a set of indicators that are able to track the human impact on a given environment (Dietz et al. 2007; Sannigrahi et al. 2017). In most of the studies, NDVI has been calculated to assess UHI/LST. Several researchers used Landsat imageries to map land use/cover and calculated temperature as well and used NDVI to describe land surface vegetation coverage (Sundara et al. 2012; Xiong et al. 2012; Lu et al. 2013). Normalized difference water index (NDWI), normalized difference built-up index (NDBI), and normalized difference bareness index (NDBaI) are considerably used indices in LST-related research works (Zha et al. 2003; Essa et al. 2012; Guha and Govil 2021a; Taloor et al. 2021). To evaluate and compare the impact of biophysical components on urban environment, NDVI, NDBI, NDWI, MNDWI, NDBal, BSI, and SAVI have been calculated in this study.

In India, medium-sized cities like Gorakhpur are also under the process of expansion and intensification. Drastic urbanization and resultant change in LU/LC have changed the thermal character of the land surface. This kind of study will help to identify the present status and trend of the land surface temperature, so that preventive measures can be formulated and implemented before the situation worsens.

Materials and methods

Methodology adopted to quantify and to assess temporal change in the land surface temperature phenomenon of Gorakhpur city and its environs includes satellite data collection, classification of images, preparation of land use/land cover maps, preparation of different maps on selected indices, quantification of temperature, and correlation of land surface temperature with land use/land cover changes (Fig. 2). ArcGIS 10.2, ERDAS IMAGINE 2010, MS Office 2016, and SPSS 20 software have been used to achieve the objectives of the study.

Data collection

This study has incorporated remotely sensed Landsat image data and applied remote sensing/digital image processing techniques to quantify the impact of urban growth on an land surface temperature of Gorakhpur city by using the data of last 28 years. Cloud-free Landsat time series satellite data of 1990, 2000, 2010, and 2019 have been downloaded from USGS Earth Explorer website (www.earthexplorer.usgs.gov). A Landsat-5TM+, 7 ETM+, and Landsat-8, OLI/TIRS image scenes (Row 142/Path 41) were selected for this study (Table 1). The multispectral image data consists of eight spectral bands (three visible, one NIR, two MIRs, and two thermals) and has a spatial resolution of 30 m for the reflective bands and 60 m for the thermal bands. Thermal infrared spectral provides data for land surface temperature measurement.

All the data have been first pre-processed and projected to the Universal Transverse Mercator (UTM) projection system. Topographic sheets of 1:50,000 scale were used for

Table 1 Details of Landsat data used

Date, year	Satellite, sensor	Path and row	Referencing system
26th February, 1990	Landsat-5, TM +	142/41	UTM and WGS84
15th February, 2000	Landsat-7, ETM +		
2nd February, 2010	Landsat-5, TM +		
8th February, 2019	Landsat-8, OLI/TIRS		

geometric corrections. The following methodologies have been adopted to quantify land surface temperature and various biophysical parameters.

Land use/land cover class extraction

The images were geometrically and radiometrically corrected, and land use/land cover maps were extracted using supervised classification with the maximum likelihood classification algorithm, which is supposed to be the most popular and useful parametric classifier. The maximum likelihood (ML) is a supervised classification method derived from the Bayes theorem, which states that the a posteriori distribution $P(i|\omega)$, i.e., the probability that a pixel with feature vector ω belongs to class *i*, is given by

$$P(i|\omega) = (P(\omega|i)P(i))/P(\omega) \tag{1}$$

where $P(\omega|i)$ is the likelihood function; $P(i)$ is the a priori information, i.e., the probability that class *i* occurs in the study area; and $P(\omega)$is the probability that ω is observed, which can be written as

$$P(\omega) = \sum_{i=1}^{M} P(\omega|i)P(i) \tag{2}$$

where M is the number of classes. $P(\omega)$ is often treated as a normalization constant to ensure sums to 1:

$$\sum_{i=1}^{M} P(i|\omega) \tag{3}$$

In this study, a land use/land cover classification scheme has been developed keeping in mind the classification system proposed by the National Remote Sensing Centre, Hyderabad, Telangana, India (NRSC, 2014). The seven land use/ land cover classes, viz., built-up, agriculture, forest, water bodies, sand, vacant land, and miscellaneous, are included in this classification system, depending on the availability of type of land use/land cover, and the area under these classes has been calculated.

Accuracy assessment

Accuracy assessment or validation is a key component of any project employing spatial data (Congalton 2001). The accuracy assessment/validation of the spatial distribution of different land use/land cover classes was done by comparing the results of classification with high-resolution images available on Google Earth, personal experience, and field samples.

Detailed field knowledge and survey conducted during studies in this area served as the bases for the estimation of accuracy of land use/land cover classification for 4 years.

Overall accuracy assessment

$$OA = \frac{Number\ of\ true\ positive\ +\ Number\ of\ true\ Negative}{Pixels\ in\ the\ ground\ truth} \times 100\% \tag{4}$$

i. User's accuracy assessment

$$UA = \frac{Rowelements_{diagonal}}{Row_{total}} \tag{5}$$

ii. Producer's accuracy assessment

$$PA = \frac{Columnelements_{diagonal}}{Column_{total}} \tag{6}$$

iii. Kappa coefficient (K)

$$K = \frac{N\sum_{1=1}^{r} x_{ii} - \sum_{i=1}^{r} x_{i+}x_{+i}}{N^2 - \sum_{i=1}^{r} x_{i+}x_{+i}} \tag{7}$$

where:

r it the number of rows/columns in confusion matrix.
Xii is the number of observations in row i and column i.
Xi + is the total number of row i.
X + *i* is the total number of column i.
N is the number of observations.

The value of *K* with more than 0.81–1 is considered as almost perfect agreement (Landis and Koch 1977 Fleiss 1981).

Biophysical components

These components are defined as a set of indicators that are able to track the human impact on the given environment (Dietz et al., 2007). To evaluate and compare the impact of biophysical components on urban environment, NDVI, NDBI, NDWI, MNDWI, NDBal, BSI, and SAVI have been calculated and mapped.

Normalized difference vegetation index (NDVI)

NDVI gives the intensity of greenness in the area and quantifies the vegetation coverage. Range of NDVI product is from − 1 to + 1. Higher values refer to healthy and dense vegetation, while lower values indicate sparse vegetation. Water and built-up areas or non-vegetative areas are represented by near zero or negative values. This index is widely used by the researchers for calculation of land surface temperature (LST) or UHI. Landsat satellite image has been used for the generation of NDVI from the red (3rd) and near-infrared (4th) bands, using the following equation:

$$NDVI = \frac{NIR - R}{NIR + R} \tag{8}$$

Normalized difference built-up index

This index serves as an indicator of surface urban heat island (SUHI) (Li et al., 2009). The normalized difference built-up index is a multispectral index established on the ratio between higher reflectance in the shortwave infrared (SWIR) region to the near-infrared (NIR) region (Lu and Weng, 2006). It is the important index to extract built-up area, i.e., impervious surfaces. This index has been used to extract built-up areas in the study region using following equation:

$$NDBI = \frac{MIR - NIR}{MIR + NIR} \tag{9}$$

Normalized difference water index

The NDWI, a remote sensing image-based indicator, is developed by Gao (1996) to enhance the water-related features of the landscapes and is used in estimating the leaf content at canopy level. According to Gao, NDWI is a good indicator for vegetation water content and is less sensitive to atmospheric scattering effects than normalized difference vegetation index. This index is derived from the near-infrared and shortwave infrared bands using the following equation:

$$NDWI = \frac{G - NIR}{G + NIR} \tag{10}$$

The range of NDWI product varies between − 1 and + 1, depending not only on the leaf water content but also on the vegetation type and cover. High NDWI (in blue) value is related to high vegetation water content and high vegetation cover, while low NDWI values (in yellow) correspond to low vegetation water content and low vegetation fraction cover. NDWI value will decrease during the period of water stress.

Modified normalized difference water index (MNDWI)

MNDWI is useful in the estimation of water bodies significantly without any built-up area and vegetation noise (Xu 2006). It is more suitable for enhancing and extracting water information for a water body with a background dominated by built-up land areas, because of its advantage in reducing and removing built-up noise over NDWI:

$$MNDWI = \frac{G - MIR}{G + MIR} \tag{11}$$

Normalized difference bareness index (NDBal)

This index can be used to derive the distribution of bare land as well as temporal study to assess the change in bare land. It can be used to monitor the anthropogenic impact:

$$NDBal = \frac{SWIR1 - TIR}{SWIR1 + TIR} \tag{12}$$

Bare soil index (BSI)

This indicator is useful in the identification of bare soil areas, vacant lands, and urban expansion as well. BSI has been calculated using the following formula:

$$BSI = \frac{(SWIR1 + R) - (NIR + B)}{(SWIR1 + R) + (NIR + B)} \tag{13}$$

Soil-adjusted vegetation index (SAVI)

The soil-adjusted vegetation index was developed as a modification of NDVI to correct the influence of soil brightness, when vegetative cover is low. Here, L is the soil brightness correction factor. Lower values indicate lower amount of green vegetation:

$$SAVI = \frac{(NIR - R)(1 + L)}{(NIR + R + L)} \tag{14}$$

Land surface temperature (LST)

The spectral radiance, converted from pixel DN values, is used to compute brightness temperature (i.e., blackbody temperature) under the assumption of unit emissivity and

using pre-launch calibration constants (Landsat Project Science Office, 2002). Using the radiance, rescaling factors are provided in the metadata file (USGS, Landsat 8 handbook, 2016). Thermal band (6th) of the Landsat Thematic Mapper 5 (TM) satellite images have been used to extract the land surface temperature, near-infrared, and red (R) for estimating vegetation health and other related information. The following methodology has been adopted to calculate land surface temperature of the study region.

Conversion of digital number (DN) to spectral radiance (Lλ) The spectral radiance (Lλ) can be given (USGS 2016) as-

$$L\lambda = L_{min\lambda} + \left[\frac{(L_{max\lambda} - L_{min\lambda})}{(Q_{CALmax} - Q_{CALmin})} \times Q_{CAL}\right] \quad (15)$$

where L is the sensor-derived spectral reflectance (W m^{-2} sr^{-1} μm^{-1}) and $L_{max\lambda}$ and $L_{min\lambda}$ are the minimum and maximum spectral radiances for band 6, respectively. Q_{CAL} is the digital number (DN) of each pixel. Q_{CALmin} is the minimum DN value of the image, here $Q_{CALmin} = 0$; and Q_{CALmax} is the maximum DN value of the image, here $Q_{CALmax} = 255$.

Conversion of spectral radiance (Lλ) to brightness temperature (Tβ) The emissivity can be computed by using the formula of Artis and Carnahan (1982):

$$T\beta = \frac{K_2}{In\left(\frac{K_1}{L_\lambda} + 1\right)} - 273.15 \quad (16)$$

where Tβ is the brightness temperature (K), Lλ represents spectral radiance of sensor (W m^{-2} sr^{-1} μm^{-1}), and K_1 and K_2 are the calibration constant ($K_1 = 60.776$ mW cm^{-2} sr^{-2} μm^{-1} and $K_2 = 1260.56$ K for Landsat band). An absolute zero (approximately − 273.15 °C) should be added to revise the temperature in terms of degree Celsius.

Emissivity correction through NDVI method This is done using following formula:

$$Pv = \left(\frac{NDVI - NDVI_{Soil}}{NDVI_{veg} + NDVI_{Soil}}\right) \quad (17)$$

where $NDVI_{soil}$ and $NDVI_{veg}$ are the threshold values of soil pixel and the pixel of vegetation. The threshold values of $NDVI_s$ are 0.2, and $NDVI_V$ is 0.7.

Land surface emissivity calculation (ϵ) The land surface emissivity (ϵ) is calculated as

$$\in \lambda = \in_{veg\lambda} P_v + \in_{soil\lambda}(1 - P_v) + C_v \quad (18)$$

where ϵ_{veg} and ϵ_{soil} are the vegetation and soil emissivity, respectively, and C is the representation of surface roughness.

Retrieval of land surface temperature After the calculation of land surface emissivity, land surface temperature is retrieved using the following formula:

$$LST = \frac{T\beta}{[1 + \{(\lambda \bullet T\beta/\rho)In \bullet \epsilon\lambda\}]} \quad (19)$$

where land surface temperature means land surface temperature in °C, $T\beta$ is the sensor brightness temperature (°C), λ is the wavelength of emitted radiance in meter ($\lambda = 10.895\ \mu m$), and $\epsilon\ \lambda$ is the emissivity:

$$\rho = h\frac{C}{\sigma} = 1.438 \times 10^{-2} mK \quad (20)$$

where σ is the Boltzmann constant (1.38×10^{-23} J K^{-1}), h is the Planck's constant (6.626×10^{-34} J K^{-1}), and C is the velocity of light (2.998×10^8 m s^{-1}).

Multiple linear regression

Multiple linear regression has been derived in the following manner:

$$y = \beta_0 + \beta_1 w_1 + \beta_2 w_2 + \beta_3 w_3 + \beta_4 w_4 + \beta_5 w_5 + \beta_6 w_6 + \beta_7 w_7$$

where:

y is the dependent variable.
β_0 is the constant.
$\beta_{(1-7)}$ is the unstandardized coefficient for each predictor variables.

Predictor variables w_1–w_7:

w_1, BSI (°C)
w_2, MNDWI
w_3, NDBal
w_4, NDBI
w_5, NDVI
w_6, NDWI
w_7, SAVI

Hot spot analysis (Getis-Ord Gi* statistics)

Hot spot analysis is used to identify the location of statistically significant hot spots and cold spots in the data by aggregating points of occurrence into polygon as points that

are in proximity to one another based on a calculated distance. It produces Z scores (Gi scores) and P values (Gi P values). Getis-Ord Gi* is calculated (Getis and Ord 1992) as

$$G_i^* = \frac{\sum_{j=1}^{n} \varphi_{i,j} xj - \overline{x} \sum_{j=1}^{n} \varphi_{i,j}}{\sqrt{\frac{n \sum_{j=1}^{n} \varphi_{i,j}^2 - \left(\sum_{j=1}^{n} \varphi_{i,j}\right)}{n-1}}} \quad (21)$$

where x_j is the attribute value for the feature j, $\varphi_{,j}$ is the spatial weight between feature i, and j,n is equal to the total number of the feature:

$$\overline{x} = \frac{\sum_{j=1}^{n} xi}{n} \quad (22)$$

and

$$S = \sqrt{\frac{\sum_{j=i}^{n} xj^2 - (\overline{x})^2}{n}} \quad (23)$$

Gi* in hot spot analysis classifies the data into range from − 3 (cold spot, 99% confidence) to 3 (hot spot, 99% confidence) with 0 being non-significant. A high Z score and small P value indicate a significant hot spot, while low negative Z score and small P value represent a significant cold spot. The higher or lower Z score shows more intense clustering of high and low value, respectively. A Z score near zero means no spatial clustering.

Study area

Gorakhpur city, one of the most important and fast expanding cities of eastern Uttar Pradesh (India), is situated in the fertile tract of Saryupar Plain, the subdivision of the Middle Ganga Plain. Gorakhpur, the administrative headquarter of North Eastern Railway (since 1954) as well as the district and divisional headquarter, is situated at the confluence of Rapti and Rohin rivers. Towards the central western end of the city, River Rohin meets River Rapti, and both these rivers form the western boundary of the city. It is situated between 26°42′ N to 26°47′ N latitude and 83°20′ E to 83°25′ E longitude (Fig. 1). Railway line passes through the middle of the city and divides it into two distinct parts northern and southern. Gorakhpur has a number of large perennial lakes, formed in most of the cases by the abandoned channels of rivers; Ramgarh lake is the biggest lake in the area. Chilika Lake and Sumer Sagar are also worth mentioning water bodies.

The city has been expanding since 1951, when it had a population of 1,32,436, which has increased to 2,30,911 in 1971, to 3,07,501in 1981, to 5,05,566 in 1991, to 6,22,701 in 2001, and finally reaching to 6.73 lakh in 2011 (source: census of India). The highest increase (64.41 per cent) was recorded between 1981 and 1991 decade, when in 1982, 47 villages were incorporated within the municipal limit. The area of interest (AOI) selected for the study area (Fig. 2) includes the surrounding non-urban area of Gorakhpur city also, so that the variation and comparison of the temperature between built-up and other land uses can easily be observed.

Results

Land use/land cover changes

Land use classification scheme has been adopted and supervised land use/land cover classification maps for the year 1990, 2000, 2010, and 2019 have been prepared, using maximum likelihood classification algorithm, and seven categories, viz., built-up, agriculture, forest, water bodies, sand, vacant land, and unclassified, have been identified. These classified images are important evidence of urban extent and also clearly identify the growth, pattern, direction, LU/LC dynamics, and spatio-temporal distribution. It is observed that Gorakhpur city has experienced rapid transformation in the land use/land cover in the last 28 years (Fig. 3, Table 2). The total area of the rectangular area of interest (AOI) is 483.97 sq. km.

An analysis, based on interpretation of land use/land cover maps of selected years, shows obvious changes in the area under built-up and vacant land. In 1990, built-up areas were limited to the middle part of the city with the expansion of 56.50 sq. km., while, in 2019, it has expanded beyond the municipal boundaries with more density and increased up to 171.56 sq. km. Thus, 23.77% increase has been noticed during this period (Table 2). Increasing demand of land for residential, industrial, educational, and other urban activities has forced the other land use classes to shrink, and the tendency of encroachment of urban land use on other types of land uses is increasing. As a result, the size of urban built-up kept on increasing. Land under agriculture, forest, sand, and water bodies has shrunk, and negative growth in all these land use classes has been noticed for the same time span. Agricultural land has experienced negative growth of about 21% and because of this tendency, agricultural land has been reduced from 313.89 sq. km in 1990 to 212.72 sq. km. in 2019.

Vacant spaces have also experienced positive growth during the study period because of the urban expansion and resulting clearing of agricultural land. This area has been left vacant sometimes for speculation and will gradually be converted into built-up area in the coming years. The built-up areas in the study area are not only densifying but also expanding almost in every direction, except the western part, where the presence of Rapti River and embankment to protect the city from annual floods has forced any built-up area to develop and less

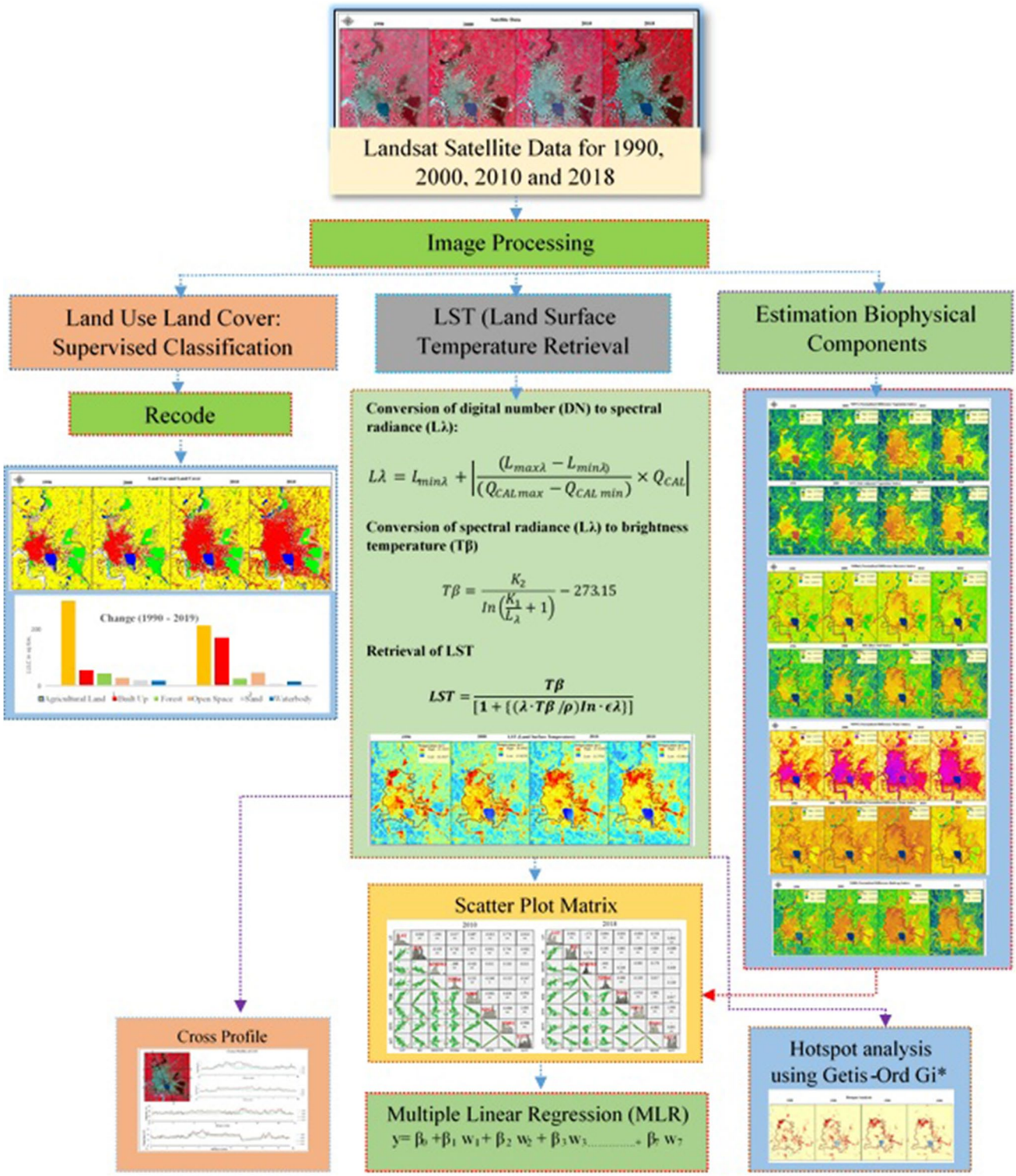

Fig. 1 Flow chart of methodology for measuring the land surface temperature

urban growth is observed particularly in the south-western part of the city. In other directions, the city growth has crossed municipal boundaries of Gorakhpur. It is also clear from the Fig. 4 that transformation of land use is mostly into built-up area from almost every land use classes during 1990–2019.

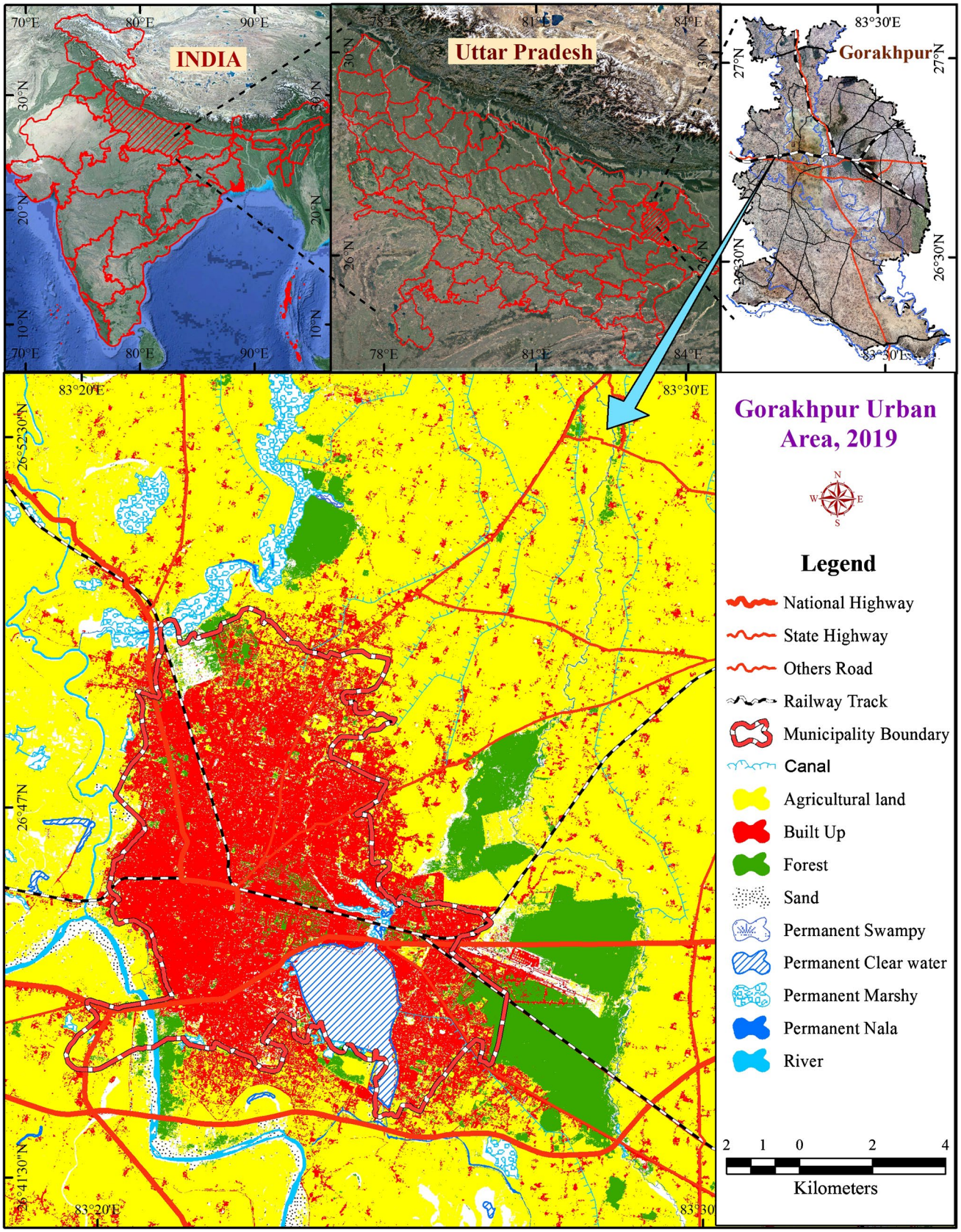

Fig. 2 Location of the study area

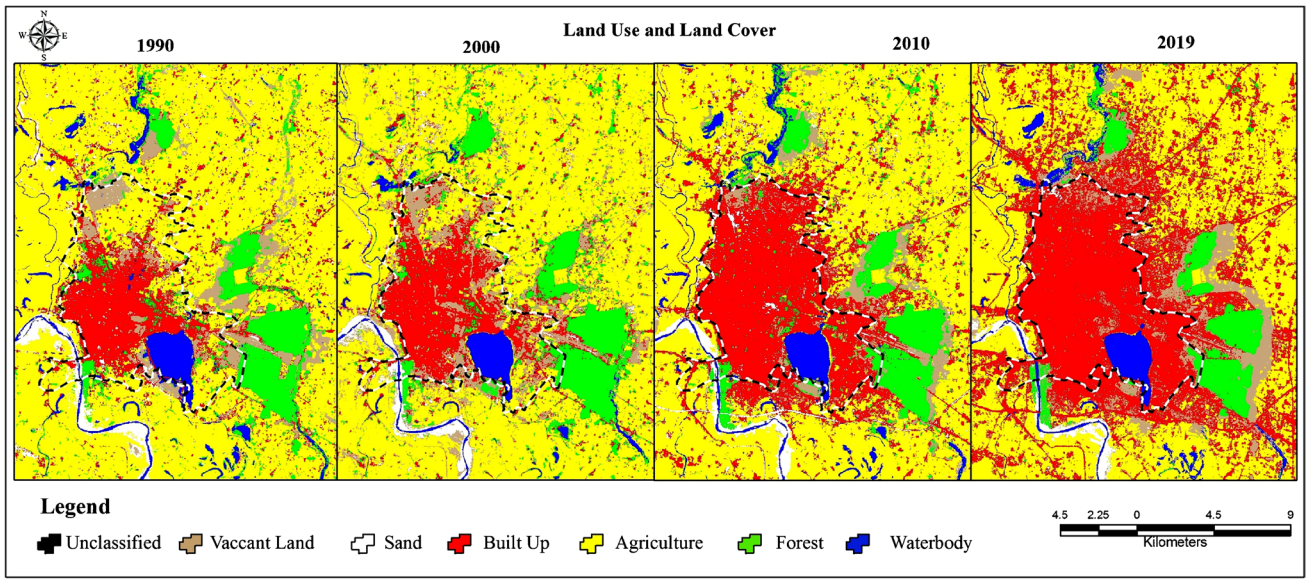

Fig. 3 Land use/land cover changes (1990–2019)

After classifying the images into different land use classes, classification accuracy has also been achieved. Table 3 shows producer's, user's, and overall accuracy and kappa coefficient of the land use/land cover classification, which has been derived using 100 control points selected by high-resolution image (Google earth images), field survey, and field knowledge of the study area. Overall accuracy is found to be between 92 and 96%, while kappa coefficient (K) value ranges between 0.864 and 0.936, which is considered an almost perfect agreement.

Biophysical components analysis

NDVI analysis

Natural vegetation provides a cooling effect on the surroundings. This clearly influences the micro-climate of any urban area. For Gorakhpur city and in its vicinity, vegetation cover is continuously decreasing due to increasing population pressure, resulting in urban expansion and land use transformation. These vegetative areas are either completely removed or converted into non-vegetative areas or their density has decreased.

In 1990, north-eastern, eastern, and south-western part of the city had high NDVI values (Fig. 5). These areas had high density of vegetation but due to urban expansion, other activities started surfacing, and gradually, non-vegetative areas started increasing, forcing the vegetative areas to shrink, and by 2019, the entire northern, north-eastern, and eastern parts (except the eastern part where reserve forest is located) were converted into the impervious surface. Only the south-western part of the city, beyond River Rapti, has sparse vegetation. In the eastern part (the reserve forest) of the city, the density of the trees has been decreasing over the years and so is the value of NDVI. Hence, the result of this is clearly seen on the land surface temperature of the area.

Soil-adjusted vegetation index (SAVI)

SAVI index maps for the years 1990 to 2019 show almost the same results as NDVI maps of the same years (Fig. 5).

Table 2 Land use/land cover changes (area in sq. km 1990–2019)

Land use/land cover	1990		2000		2010		2019		Rate of change from 1990 to 2019 in %
	Area	% of area	Area	% of area	Area	% of area	Area	% of area	
Agricultural land	313.89	64.86	288.62	59.64	258.66	53.45	212.72	43.95	−20.90
Built-up	56.50	11.68	57.78	11.94	117.49	24.28	171.56	35.45	+23.77
Vegetation	44.22	9.14	52.79	10.91	40.08	8.28	26.88	5.55	−3.58
Vacant land	29.51	6.10	58.62	12.11	29.24	6.04	47.29	9.77	+3.67
Sand	20.80	4.30	13.05	2.70	20.37	4.21	8.81	1.82	−2.48
Water body	19.04	3.93	13.11	2.71	18.14	3.75	16.71	3.45	−0.48
Total	483.97	100	483.97	100	483.97	100	483.97	100	0

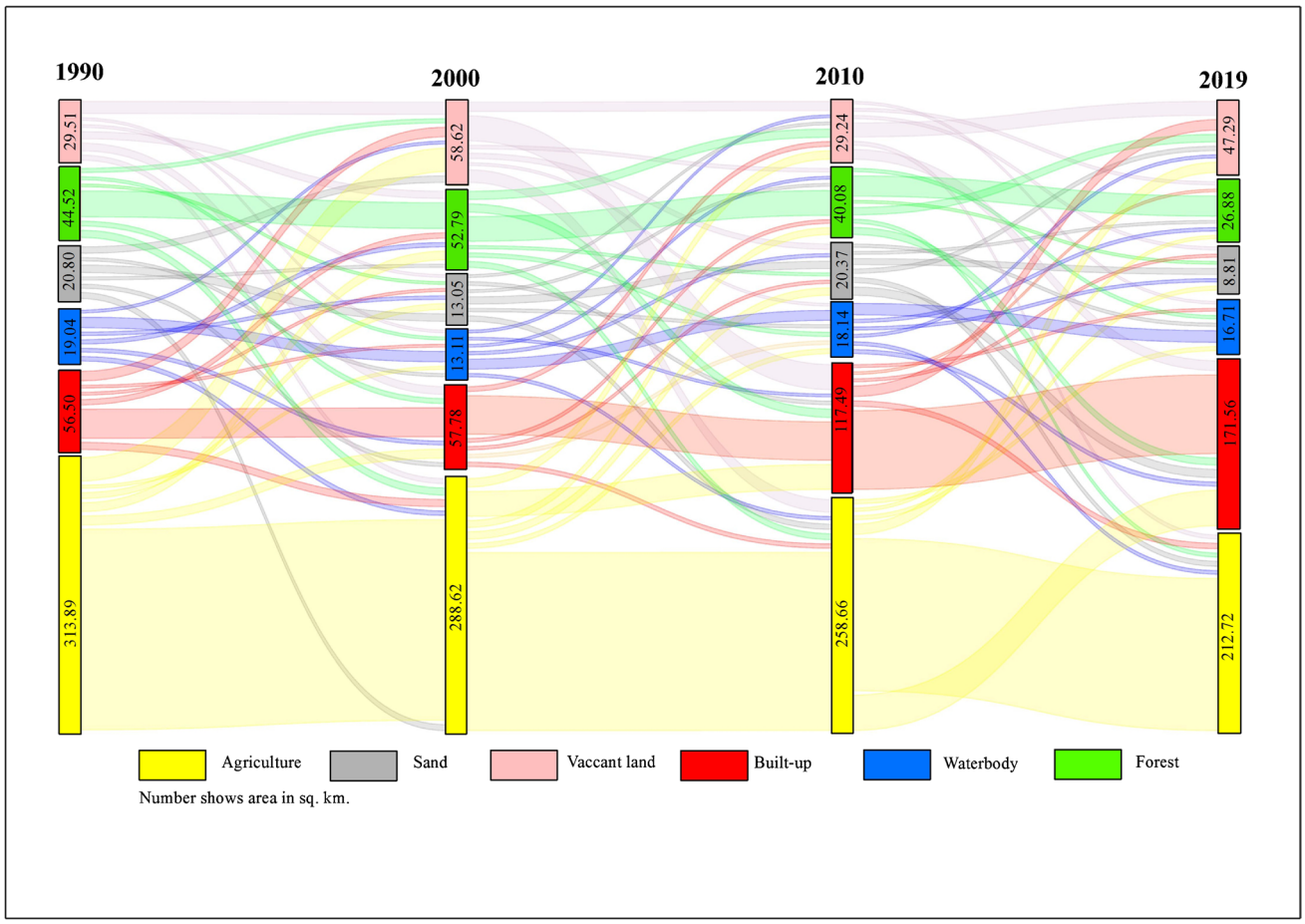

Fig. 4 Land use/land cover change trajectories (1990–2019)

Table 3 Classification accuracy assessment

Land cover class	Producer accuracy in per cent				Users accuracy in per cent			
	1990	**2000**	**2010**	**2019**	**1990**	**2000**	**2010**	**2019**
Vacant land	100	100	66.67	100	80	69.23	100	50
Sand	100	100	100	100	33.3	100	100	100
Built-up	77.78	80	93.94	90.63	100	94.12	94.23	93.55
Agriculture	98.39	100	100	96.36	96.83	98.15	100	94.64
Forest	100	91.67	100	60	100	100	96.8	100
Waterbody	100	75	100	75	100	100	100	100
Overall accuracy	95	94	96	92				
Kappa coefficient	0.9123	0.9082	0.9363	0.864				

Lower values are found in the areas of the city, where lower NDVI values have been observed. Spatial distribution and intensity of lower values are increasing with the time and following the distribution pattern of NDVI.

Normalized difference built-up index

It is the most important and widely used technique to measure the spectral signature of the urban built-up and to extract built-up area class, i.e., impervious surface in the land use classification. City expansion trend can also be assessed by applying this index on temporal data. The difference in impervious surface cover is determined by raster subtraction for monitoring the changes.

NDBI images for the study region are prepared for the year 1990, 2000, 2010, and 2019 (Fig. 6). In 1990, the city expansion was limited to the mid-western part of the city, and large stretch of agriculture land was available on the north-eastern part and to some extent in the eastern part of the city. In 2008, the built-up expansion of the city started

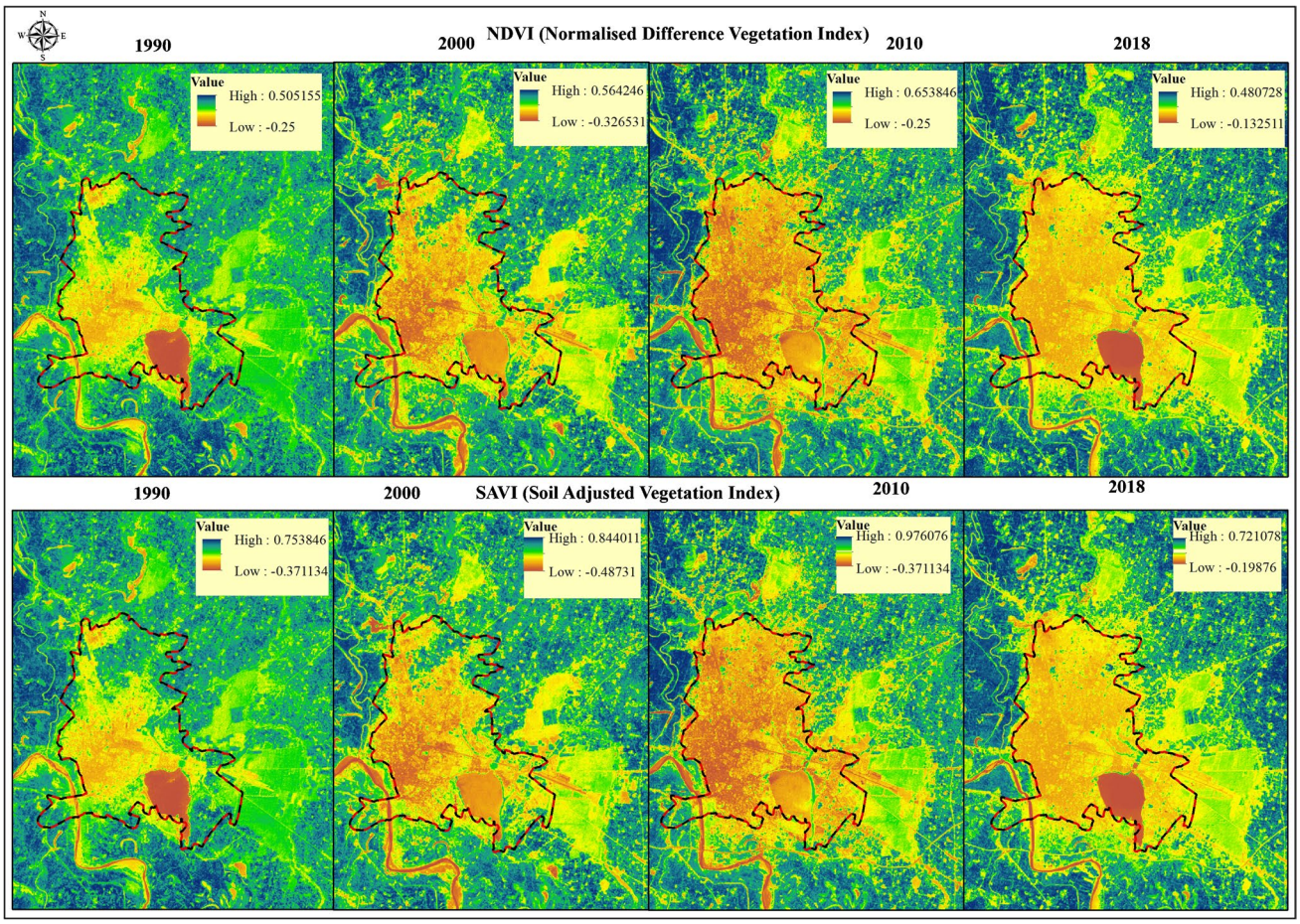

Fig. 5 NDVI and SAVI Index

to encroach this green area. In 2010, almost every part of the land within the city limit, except the south-western corner, had been converted into the impervious surface, and in 2019, it has expanded beyond the city municipal boundary, particularly in the north-east region and along the southern boundary.

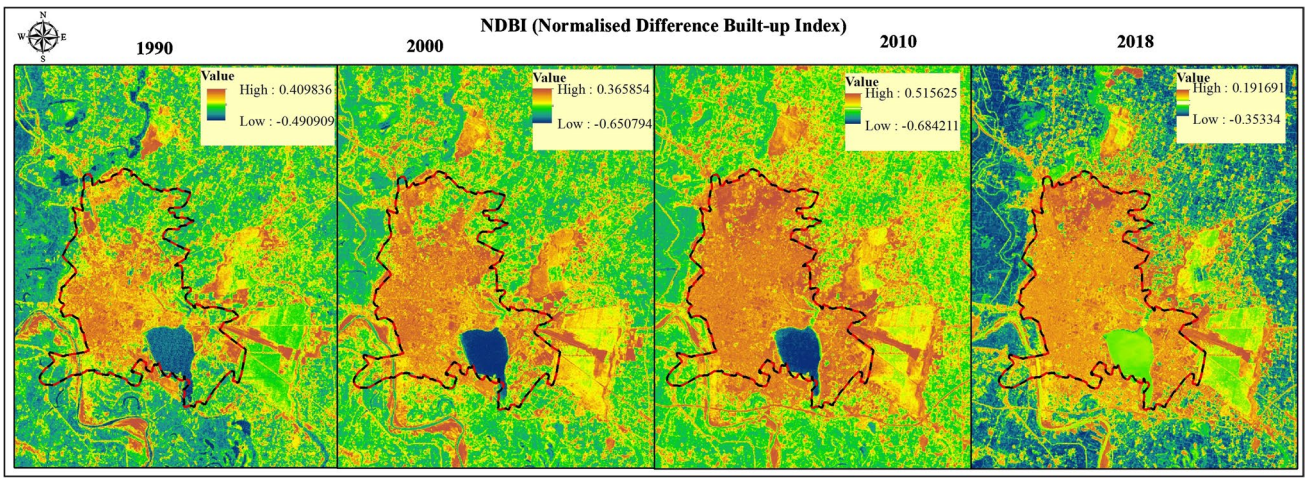

Fig. 6 Normalized difference built-up index (NDBI)

Normalized difference water index

NDWI shows the water content of leaves and is considered a better indicator than NDVI. This index for the study area shows that the highest value, which should be below one, is continuously decreasing. In 1990, it was 0.33, which has reduced to 0.17 in 2019. This trend is the clear indicator that vegetation cover is shrinking due to expansion of built-up areas. The areas of high value are also reducing, which is very clearly seen in the map of 2010 and 2019 (Fig. 7).

Modified normalized difference water index (MNDWI)

This index clearly identifies and demarcates the water bodies, situated within the built-up areas. Comparison of the maps prepared through this index, which shows the effect of urban expansion, is clearly visible on the water bodies. The biggest water body is located in the south-eastern part of the city. The western margin of this water body shows the reduction in size, which has been either converted into built-up areas or filled and left as vacant land for future development (Fig. 7). Even houses located at the bank of north-west margin are continuously filling the land and converting the water bodies into residential areas due to poor monitoring of the administration.

Normalized difference bareness index (NDBal)

Bareness index identifies the distribution and changes in bare land and is associated with high values. Bare land shows increasing trend (Fig. 8). Particularly the outer areas of old city. north-eastern, and southern parts of the city have exhibited increasing values and spatial expansion with the time.

Bare soil index (BSI)

Urban expansion results in the removal of vegetation or encroachment of agricultural land and convert these areas into vacant land. BSI for Gorakhpur city for the year 1990, 2000, 2010, and 2019 shows that the areas of high BSI are continuously increasing. In 1990, the northern part of the city having the low BSI value has been transformed into high BSI values in 2019 (Fig. 8).

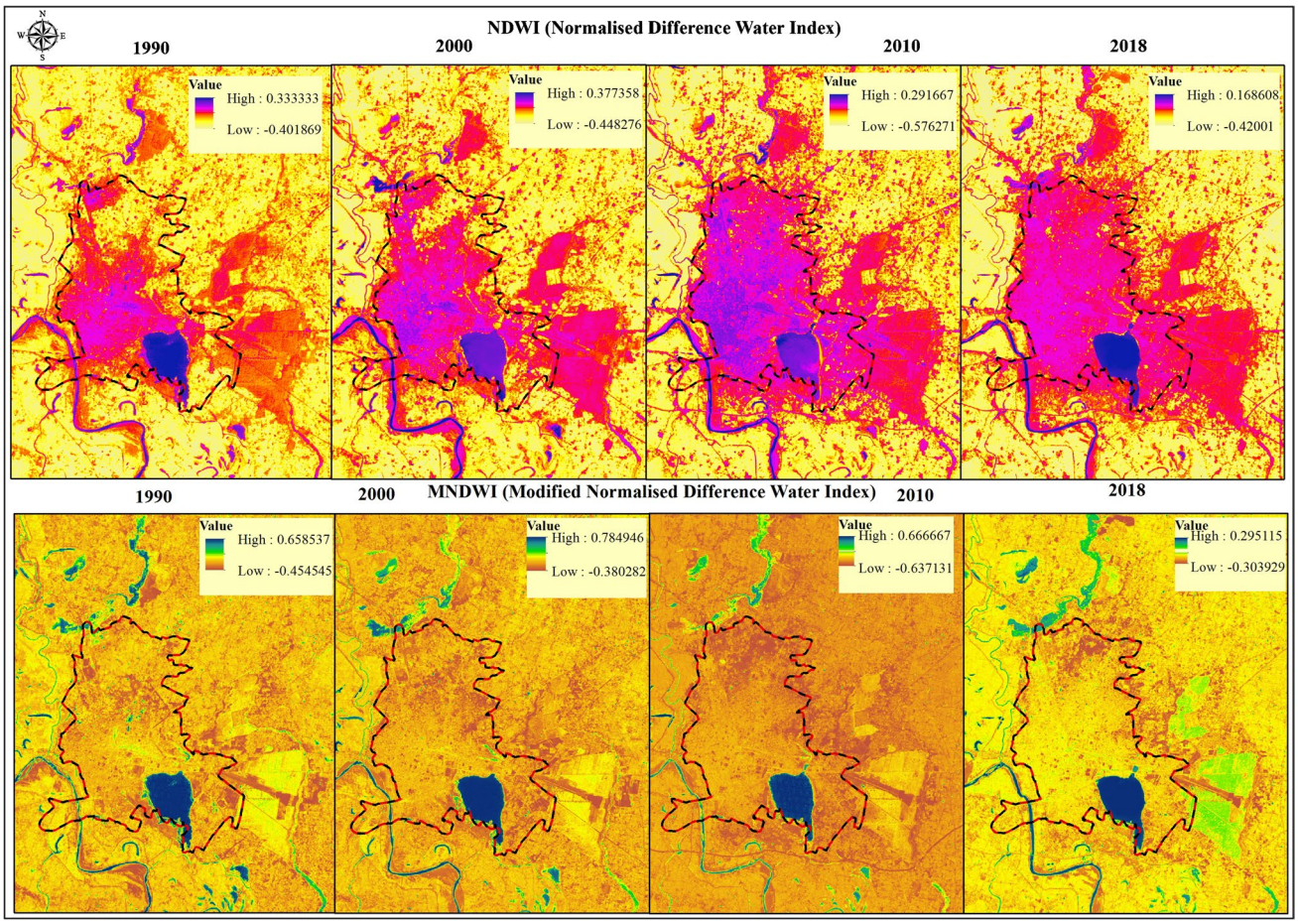

Fig. 7 NDWI and MNDWI index

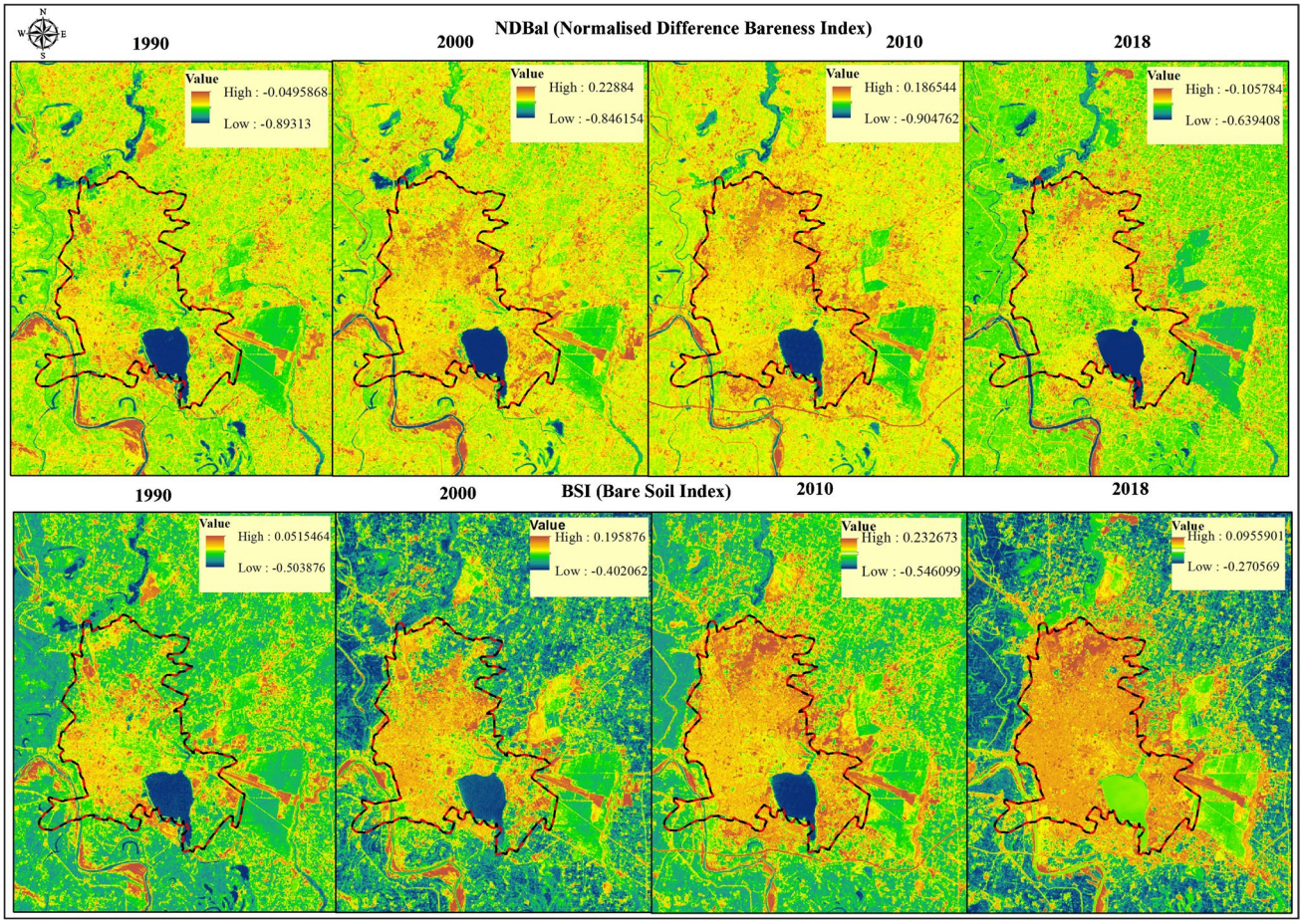

Fig. 8 NDBal and BSI index

Land surface temperature pattern and statistics

From brightness temperature (TB) and emissivity images, the final land surface temperature (LST) maps for four years have been generated by using algorithms of ERDAS Imagine 10. The spatial and temporal distribution trend of land surface temperature during 1991–2019 in the study area is shown in Fig. 9, which indicates that remarkable increase in land surface temperature has been observed in the northern part of within the municipal boundary and in the eastern part outside the city limit.

Multiple linear regression

The multiple linear regression analysis has been used to find out the relationship between independent and dependent variables, and their effect on the pattern of land surface temperature has also been assessed. Multiple linear regression can also be used to predict future pattern of land surface temperature. In this study, variables like BSI, MNDWI, NDBal, NDBI, NDVI, NDWI, and SAVI have been used for the selected four time periods to assess the status of land surface temperature with the changeability of biophysical parameters.

The correlation coefficient of the year 1990 is $R = 0.732$, and the coefficient of determination $R^2 = 0.536$, i.e., 53.60%, and the predicted $R^2 = 50.1\%$ (Table 6). It means, this year land surface temperature was not much affected, as the built-up area was less, and significant area existed under vegetation cover and water bodies. But the results of later years indicate significant correlation coefficient among the variables (60% to 82%). The correlation coefficient of the year 2000 is $R = 0.829$, and the coefficient of determination $R^2 = 0.688$, i.e., 68.80%, and the predicted $R^2 = 66\%$. Similarly, in 2010, the correlation coefficient is 0.873, and the coefficient of determination $R^2 = 0.763$, i.e., 76.30%, and the predicted R^2 is 74.5%. The R value for the year 2019 is 0.905, and R^2 is 0.82, i.e., 82%, and the predicted R^2 is 80.6%, which show that the selected biophysical variables are significantly controlling and defining the patterns and distribution of land surface temperature. Thus, the study explains that rapidly increasing built-up areas and decreasing

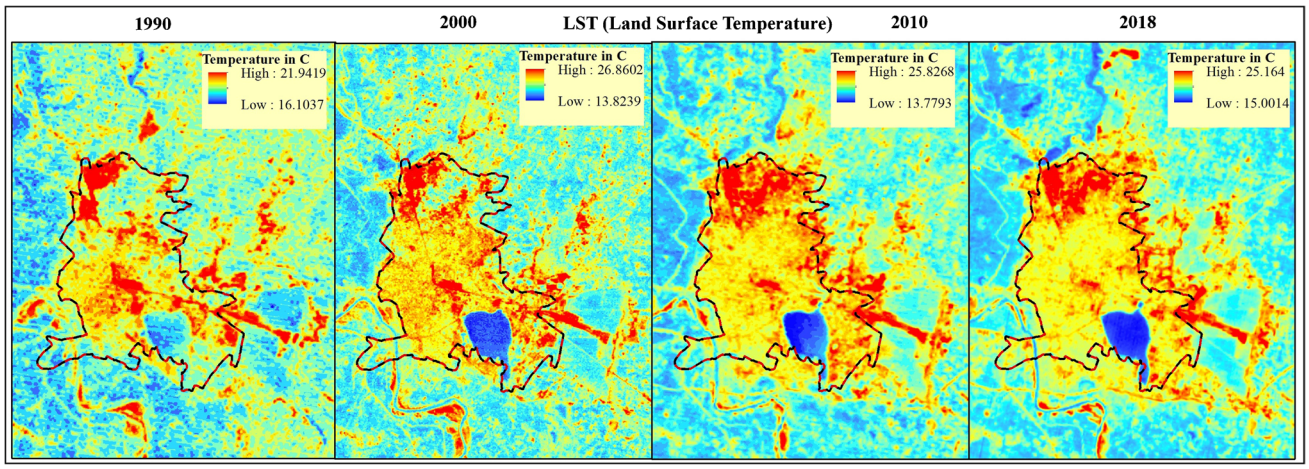

Fig. 9 Land surface temperature (1990–2019)

vegetation cover and water bodies are gradually increasing the land surface temperature in the study area.

Hot spot analysis

The identification of the hot spots helps to identify areas of priority for the implementation of mitigation and adaptation strategies. Hot spot maps using Getis-Ord-Gi* statistics for the selected years to highlight the hot spot and cold spot areas in Gorakhpur Urban Area have been produced. It is based on mean land surface temperature derived from remotely sensed data. From the statistical results, the land surface temperature pattern has been divided into seven categories.

The expanding heat island is clearly visible during the 18-year change analysis. Significant hot spots of high land surface temperature were recorded in built-up areas, industrial areas, and bare surfaces, while significant cold spots were seen on vegetated surfaces and water bodies. In general, the land surface temperature, hot spots, and cold spots were shown to have been greatly influenced by the LU/LC of the area.

Statistically significant hot spots and their spatial distribution show that high hot spot areas are scattered in small clusters in the northern part of the municipal area (Fig. 10), and their areal distribution shows gradually expanding trend. In 1990, this hot spot was confined to the north-west part of the city only, but in later years, it has almost covered the northern part of the municipal area. Airport, situated in the south-eastern part of the city, also falls in the very high hot spot category. Railway workshop, situated in the middle part, shows diminishing trend because of increasing greener cover. Hot spots and warm spots are also distributed in the vicinity of very high spot. Water body (Ramgarh lake) shows up as a very cold spot. Other small water bodies scattered in the area are in cold and cooler spots. These water bodies have positive impact in reducing the urban thermal environment.

Discussion

It is obvious from the results of the present study that LU/LC and biophysical parameters are significant to address the dynamic pattern of LST of an urban landscape due to anthropogenic activities. The analysis of images of land surface temperature in Gorakhpur city shows that high temperature areas correspond to areas with no vegetated cover, while vegetated surfaces and water bodies recorded a relatively low temperature. The northern part of the city exhibits increasing trend in the temperature and spatial distribution as well. In 1990, the northwestern part, which is an industrial area of the city, railway station, and nearby railway workshop area, and the densely populated areas of the city have recorded the highest temperature.

Spatial distribution pattern of land surface temperature (LST) in 2010 and 2019 shows that the northern part of the city was under high temperature zone. The eastern part where airstrip is located inside the forest area and central part is also among the high-temperature areas.

The number of the highest land surface temperature areas kept on increasing, and the whole northern and eastern areas, at the periphery of the municipal boundary, are included in this category, whereas Ramgarh Lake is the coolest area of the city. Thus, this area is generating cooling effect on the urban micro climate. Central, western, and the south-western parts also have higher temperature. Thus, high temperature is associated with industrial activities, impervious surface, and other urban activities, while water bodies and vegetative areas are directly

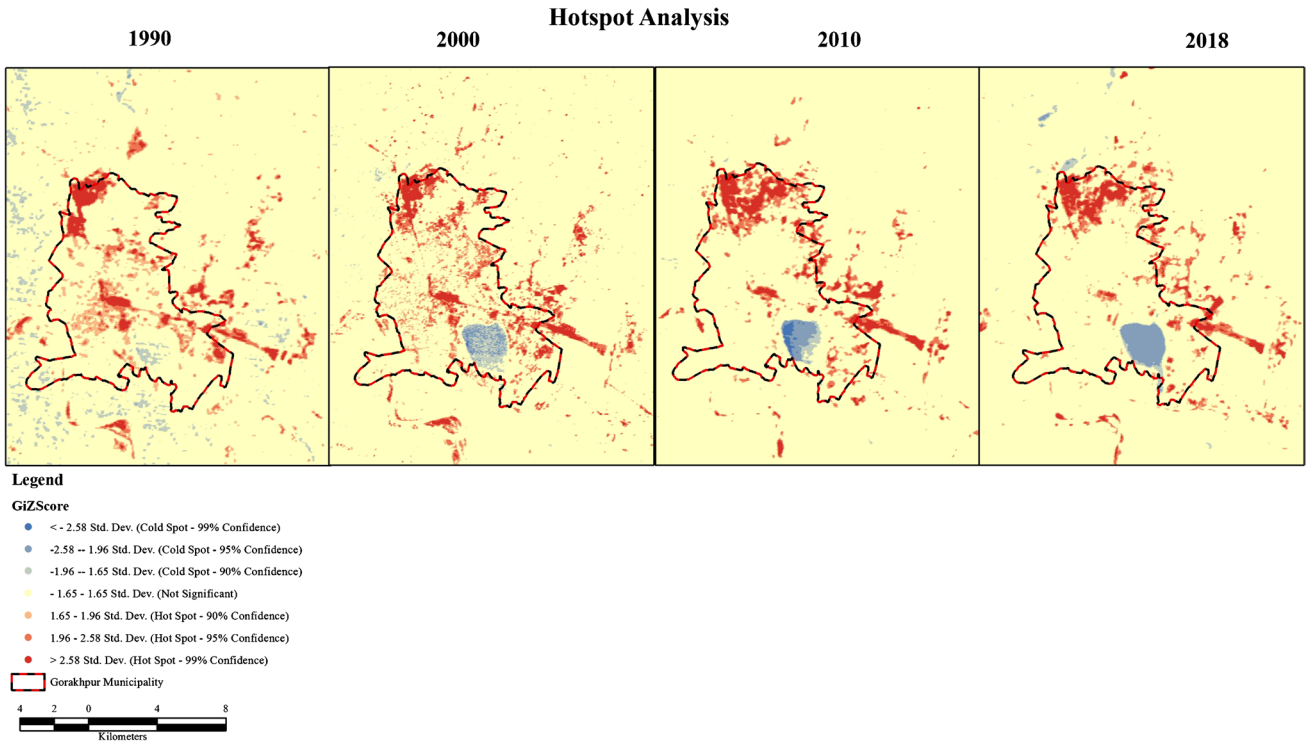

Fig. 10 Hot spots of year 1990, 2000, 2010, and 2019

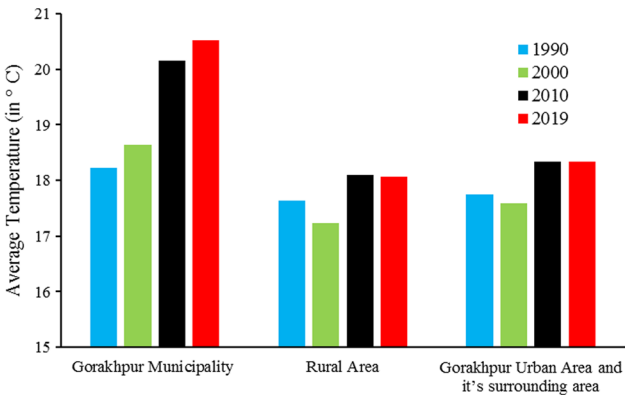

Fig. 11 Average LST in Gorakhpur city (1990–2019)

related to the lower land surface temperature. Vegetation and evapotranspiration help in lowering both surface and air temperatures (Adeyeri and Okogbue 2014).

The average land surface temperature of the study area is continuously rising during 1990–2019 (Fig. 11 and Table 4). The highest change has been observed within the municipal areas. In 1990, the average land surface temperature was 18.22 °C, but in 2019, with the increase of more than 2 °C, it reached up to 20.52 °C. Thus, in the last 28 years, overall, there is an increase of 2.3 °C in land surface temperature of Gorakhpur city. Moderate change in the temperature occurred in the neighboring urban areas, located outside the municipal limits. Here, 0.59 °C temperature increase has been observed. Not much difference in the land surface temperature is noticed in the rural areas. Here, only 0.44 °C increase in the temperature is recorded. Thus, land surface temperature pattern is strongly correlated with the land use/land cover class distribution. The temperature profiles and average increase in land surface temperature clearly demonstrate the urban heat island effect in some parts of the study area.

Table 4 Multiple linear regression for land surface temperature and biophysical parameters, 1990 to 2019

Year	Regression equation	R	R^2	Adjusted R^2	P value
1990	LST = 16.340 + 3.99 BSI + 6.005 MNDWI − 4.503 NDBal + 8.154 NDBI + 3.054 NDVI − 13.15 NDWI − 5.693 SAVI	0.732	0.536	0.501	0.0001
2000	LST = 16.628 + 19.239 BSI − 3.272 MNDWI − 12.170 NDBal + 2.424 NDBI + 5.345 NDVI − 11.077 NDWI − 6.024 SAVI	0.829	0.688	0.664	0.0001
2010	LST = 17.604 + 3.567 BSI − 10.219 MNDWI − 3.892 NDBal − 2.780 NDBI + 13.087 NDVI + 5.310 NDWI − 11.278 SAVI	0.873	0.763	0.745	0.0001
2019	LST = 12.438 + 8.175 BSI − 16.196 MNDWI − 16.053 NDBal + 1.8 NDBI − 0.970 NDVI − 26.193 NDWI − 15.918 SAVI	0.905	0.82	0.806	0.0001

Four transacts, three from west to east and one passing through north-west to south-east part of area of interest (AOI), were drawn (Fig. 12). These lines pass through almost all types of land use/land cover classes. Along these lines, temperature profiles are created, and it has been observed by the analysis of these transacts that in 2010, the highest temperature of about 22.86 °C exists on urban built-up area, which represents intense concrete areas; 24.56 °C on vacant land, which has been converted from agricultural land; and 24.55° C on industrial and other impervious surfaces. In 2019, agricultural areas show relatively low temperature of about 16.6 °C; the lowest temperature 15.06 °C has been observed at Ramgarh Lake areas due to the availability of vast stretch of water. Thus, peaks of the temperature correspond to the built-up and vacant land.

A linear regression using Pearson's correlation analysis has been carried out to evaluate the correlation of land surface temperature (LST) with the seven indices with 100 sample points (Fig. 12). Land surface temperature is positively correlated with some indices, while it is negatively correlated with others depending on the type of LU/LC classes (Sannigrahi et al. 2017). Land surface temperature has strong positive correlation with BSI and NDBI, which show the contribution of impervious surface on heat island or hot spot formation. The value of relationship of these two parameters ranges between 0.646 in 1990 to 0.842 in 2019 and 0.689 in 1990 to 0.830 in 2019, respectively (Table 5), which is in accordance with the results of Wuhan city, China (Chen et al. 2013). Land surface temperature has moderate positive correlation with NDBal and NDWI. The values of correlation of coefficient also show a gradually increasing trend. Nimish and Bharath (2020) established a correlation between LST and a NDBaI in Kolkata Metropolitan Area, India. The correlation of land surface temperature with NDVI, MNDWI, and SAVI exhibit a negative trend.

NDVI values tend to become weaker with the increase in built-up area. These areas normally have high NDBI and BSI.

Study on the impact of land use changes on land surface temperature in Lagos, Nigeria, between 2002–2013 showed that land surface temperature has increased with urban growth and density of urban area. Non-vegetative areas had higher land surface temperature (Imnoff et al., 2010). This has a negative impact on the ecosystem and human health. In the past, many studies found a negative correlation between land surface temperature and NDVI (Kustas et al., 2003; Agam et al., 2007; Inamdar et al., 2008) (Table 6).

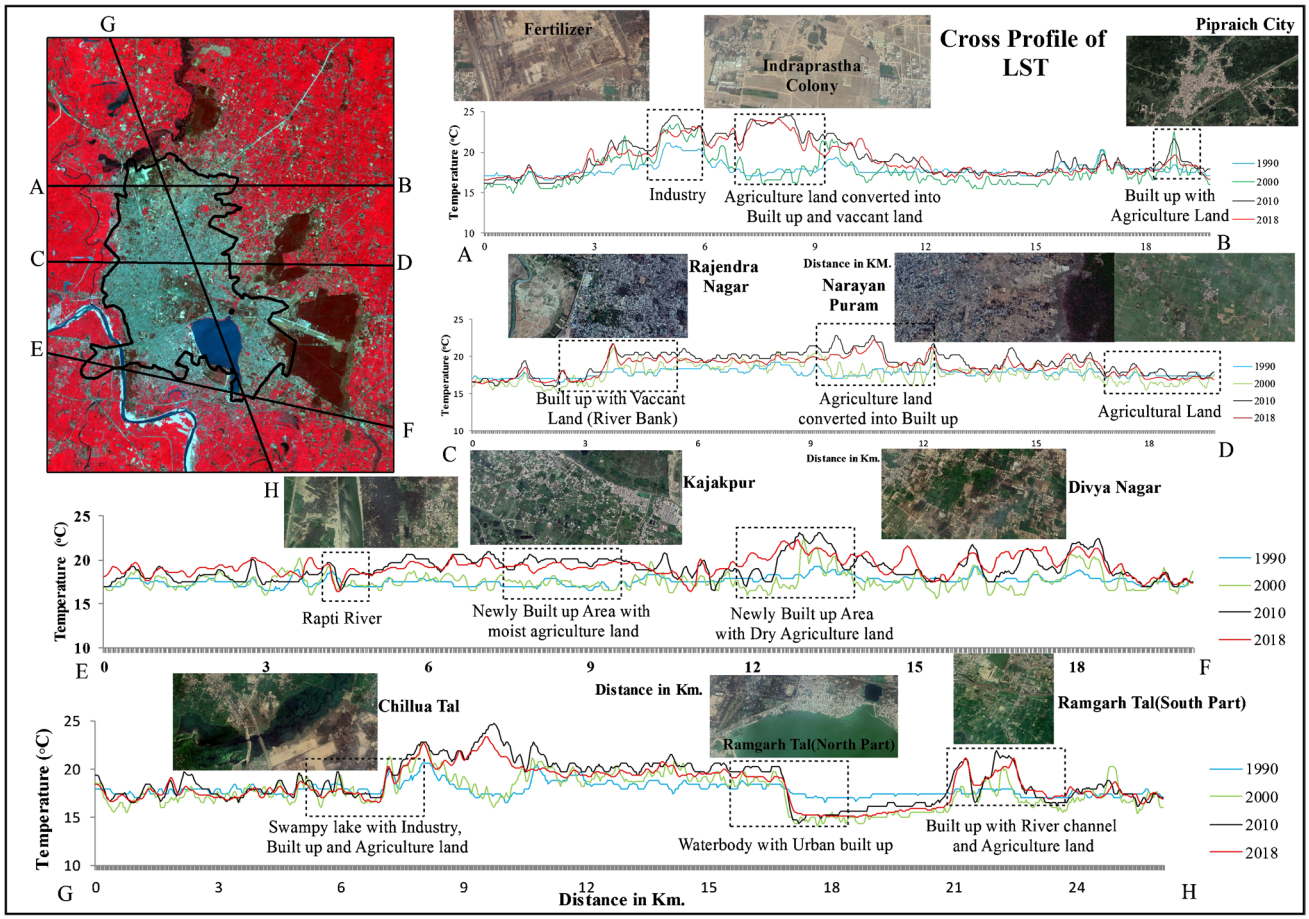

Fig. 12 Land surface temperature: cross-profile of 1990, 2000, 2010, and 2019

Table 5 Average LST in Gorakhpur city, 1990–2019

Year	Average temperature (LST)		
	Gorakhpur municipality	Rural area	Gorakhpur urban area and its surrounding area
1990	18.22 °C	17.63 °C	17.74 °C
2000	18.64 °C	17.23 °C	17.59 °C
2010	20.16 °C	18.10 °C	18.34 °C
2019	20.52 °C	18.07 °C	18.33 °C
Change from 1990 to 2019	2.3 °C	0.44 °C	0.59 °C

Table 6 Correlation coefficient for the biophysical parameters and LST for the year 1990 to 2019

Biophysical parameters	Coefficient of correlation			
	1990	2000	2010	2019
BSI	.646**	.800**	.826**	.842**
MNDWI	−.352**	−.510**	−.308**	−.578**
NDBal	.389**	.585**	.417**	.644**
NDBI	.689**	.809**	.867**	.830**
NDVI	−.515**	−.621**	−.813**	−.639**
NDWI	.436**	.511**	.778**	.558**
SAVI	−.515**	−.621**	−.814**	−.641**

*Correlation is significant at the 0.05 level (2-tailed)

**Correlation is significant at the 0.01 level (2-tailed)

Mallick et al. (2008) estimated land surface temperature over Delhi using Landsat-7 ETM+, while a comparative study carried out in Mumbai and Delhi revealed that the intensity of the UHI has increased due to the alteration of vegetation cover caused by urban development. The study concludes that there is a strong negative correlation between NDVI and UHI. Mumbai had more UHI than Delhi. The validation of the heat island is done in relation to the normalized difference vegetation index pattern. The study concludes that there exists a strong negative correlation between NDVI and UHI. Mumbai had more UHI than Delhi (Grover and Singh, 2015).

Weng et al. (2004) derived the vegetation fraction from Landsat ETM+ images and found a stronger negative correlation between land surface temperature than NDVI. Yuan and Bauer (2007) made a similar analysis, but they correlated the fraction of impervious surface area (ISA) that shows strong positive correlation to the land surface temperature in urban areas. The impervious nature of LU/LC class and surface roughness also has a role to play in the UHI creation (Li et al., 2011; Yuan and Bauer 2007; Zhou et al. 2011; Sharma et al. 2015; Wang et al. 2018).

In order to analyze the correlation between land surface temperature and selected seven indicators, scatter plots are drawn (Fig. 13). The trend analysis of land surface temperature against different land use/land cover (LU/LC) indicates that land surface temperature increases with a decrease in vegetation cover, while it increases as the built-up area increases. Thus, parks, playgrounds, and water bodies are the land surface temperature reducing surfaces. This observation is very similar to previous studies (Liu and Zhang 2011; Guo et al., 2016; Guha and Govil 2021b).

Conclusion

The study is aimed to evaluate the nature of urban growth and its impact on land use transformation and ultimately its contribution on the overall increase in the land surface temperature of Gorakhpur city and its environs. During the study period, urban built-up area has increased from 11.68to 35.45%, and thus, 23.77% overall increase has been observed. Vacant land has also experienced increasing trend. The rest of the land use classes showed negative growth. It is necessary to understand spatial distribution of land surface temperature and its relation with different types of land use/land cover to mitigate the urban heat island effect. On one hand, it will help to know the extent of hot spots and their intensity, while on the other hand, it will also help to plan strategies accordingly and more effectively. Getis-Ord-Gi* statistics has been utilized to understand the spatio-temporal dynamics of land surface temperature. The expanding heat island is clearly visible in the northern and outside the north-eastern boundary of the city.

The study clearly indicates that land surface temperature significantly varies with the variation of biophysical variables. High correlation is found between biophysical parameters and land surface temperature. The highest correlation is observed in BSI and NDBI with land surface temperature ($R = 0.842$ and 0.830, respectively). Vegetative and non-vegetative areas play important role in the modification of land surface temperature. An effective way to buffer environmental temperature in a city is to increase vegetated surfaces (Anyanwu and Kanu, 2006; Adeyeri and Okogbue, 2014). Areas having high land surface temperature have been clearly identified by the study. The northern part of the city (an industrial area of the city) and the middle part need immediate attention to decrease the temperature.

This study concludes that high temperature areas are located in scattered pattern and related to certain types of land use such as built-up and vacant. Rapidly increasing built-up areas, industrial activities, diminishing agricultural activities, decreasing vegetation cover, and shrinking water bodies are the main factors responsible for the present increasing trend of land surface

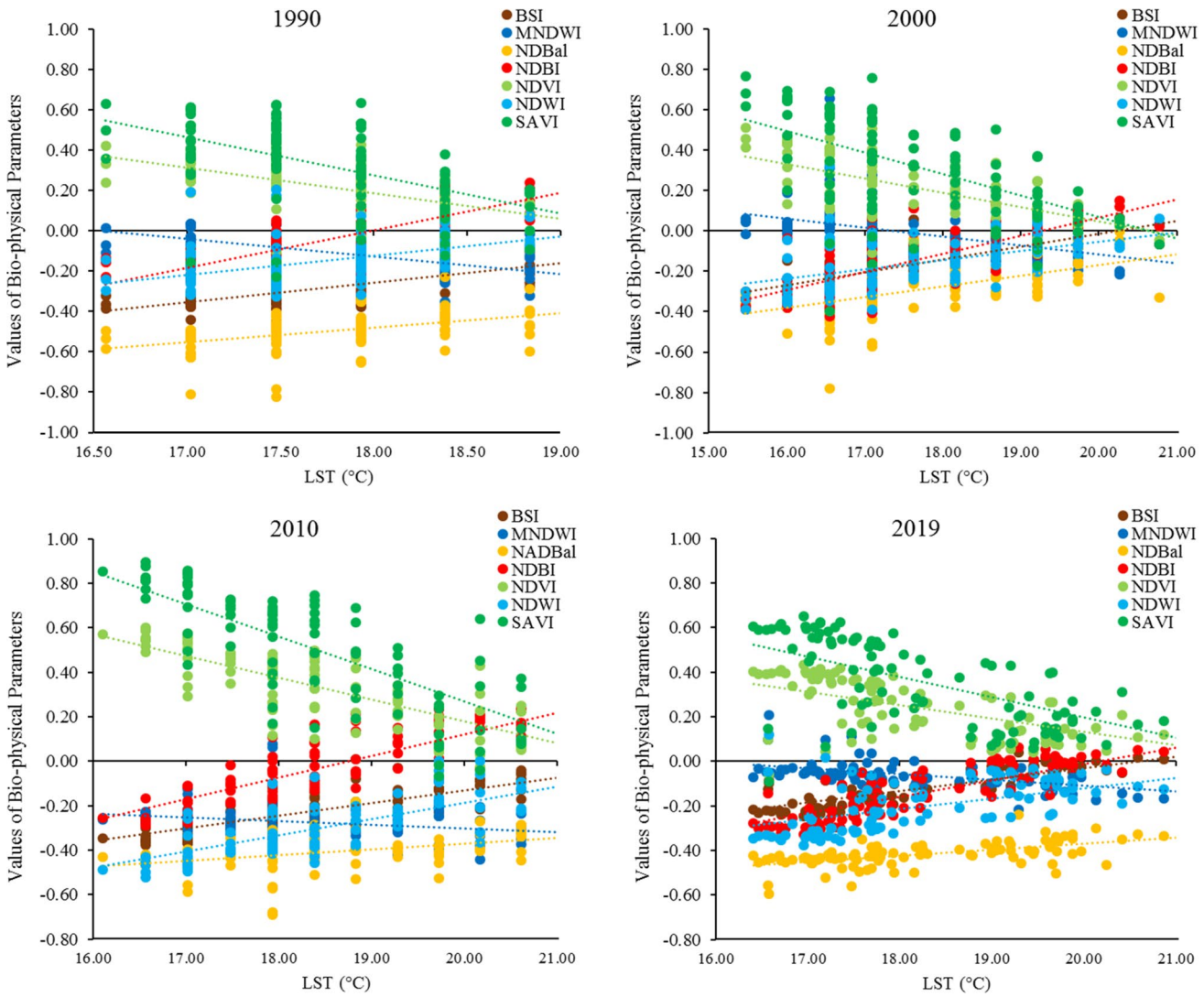

Fig. 13 Scatterplot of LST and biophysical parameters

temperature. This has adversely affected various biophysical parameters. Therefore, this kind of study and implementation of policies according to the plan will ensure the healthy and sustainable development of urban areas. Tree plantation drive and conservation of green spaces will be useful in reducing the land surface temperature and local climate as a whole. Comprehensive greening plan needs to be taken on zonation basis, and first priority should be given to high hot spot areas. Reduction of excessive heat surfaces, anthropogenic heat, and increase in shading and evapotranspiration will help in the improvement of local thermal environment. Efforts should be made to increase greenery in thickly populated urban areas through regulations. The results of this study will provide information and guidance to urban planners, administrators, and other authorities to understand the ground situation in a better way. So that they can draft their plan to reduce the land surface temperature in future on priority basis. Better urban planning and regulations can prevent further increase of land surface temperature and heat island phenomena in Gorakhpur city.

Data availability The datasets generated during and/or analyzed during the current study are available from the corresponding author on reasonable request.

Declarations

Conflict of interest The authors declare no competing interests.

References

Adeyeri OE, Okogbue E (2014) Effect of land use/land cover on land surface temperature in Abuja using remote sensing and geographic information system (GIS), in proceedings of the climate change and sustainable economic development, Nov. 9th -12th :175–184

Agam N, Kustas WP, Anderson MC, Li F, Neale CM (2007) A vegetation index-based technique for spatial sharpening of thermal imagery. Remote Sens Environ 107(4):545–558

Amiri R, Weng Q, Alimohammadi A, Alavipanah SK (2009) Spatial-temporal dynamics of land surface temperature in relation to fractional vegetation cover and land use/cover in the Tabriz urban area, Iran. Remote Sens Environ 113:2606–2617

Anyanwu EC, Kanu I (2006) The role of urban forest in the protection of human environmental health in geographically prone unpredictable hostile weather conditions. Int J Environ Sci Technol 3:197–201

Artis DA, Carnahan WH (1982) Survey of emissivity variability in thermography of urban areas. Remote Sens Env 12(4):313–329

Chen L, Huang M, Li F, Xu S (2013) Relationships of LST to NDBI and NDVI in Wuhan City Based on Landsat ETM+ image, 6th International Congress on Image and Signal Processing (CISP), Hangzhou: 840–845

Congalton RG (2001) Accuracy assessment and validation of remotely sensed and other spatial information. Int J Wildland Fire 10:321–328

Dietz T, Rosa EA, York R (2007) Driving the human ecological footprint. Front Ecol Environ 5(1):13–18

Dontree S (2010) Relation of land surface temperature (LST) and land use/land cover (LU/LC) from remotely sensed data in Chiang Mai-Lamphun basin, in SEAGA conference, Hanoi, Vietnam

Essa W, Verbeiren B, Kwast J, Van der, Voorde T. Van de, Batelaan O. (2012) Evaluation of the DisTrad thermal sharpening methodology for urban areas. Int J Appl Earth Obs Geoinf 19:163–172

Fleiss JL (1981) Statistical methods for rates and proportions, 2nd edn. John Wiley, New York

Gao BC (1996) NDWI - a normalized difference water index for remote sensing of vegetation liquid water from space. Remote Sens Environ 58:257–266

Getis A, Ord JK (1992) The analysis of spatial association by use of distance statistics. Geogr Anal 24:189–206

Grover Aakriti and Singh Ram Babu (2015) Analysis of urban heat island (UHI) in relation to normalized difference vegetation index (NDVI): a comparative study of Delhi and Mumbai. Environments 2:125–138

Guha S, Govil H (2021a) Annual assessment on the relationship between land surface temperature and six remote sensing indices using Landsat data from 1988 to 2019. Geocarto Int 1886339

Guha S, Govil H (2021b) Relationship between land surface temperature and normalized difference water index on various land surfaces: a seasonal analysis. Int J Eng Geosci 6(3):165–173

Guo G, Zhou X, Wu Z, Xiao R, Chen Y (2016) Characterizing the impact of urban morphology heterogeneity on land surface temperature in Guangzhou China. Environ Model Softw 84:427–439

Igun E, Williams M (2018) Impact of urban land cover change on land surface temperature. Global J Environ Sci Manage 4(1):47–58

Imnoff ML, Zhang P, Wolfe RE, Bounoua L (2010) Remote sensing of the urban heat island effect across biomass in the continental USA. Remote Sens Environ 114:504–513

Imran HM, Hossain A, Saiful Islam AKM, Rahman A, Bhuiyan Md A E, Paul S, Alam A (2021) Impact of land cover changes on land surface temperature and human thermal comfort in Dhaka city of Bangladesh. Earth Syst Environ 5:667–693

Inamdar AK, French A, Hook S, Vaughan G, Luckett W (2008) Land surface temperature retrieval at high spatial and temporal resolutions over the south-western United States. J Geophys Res 113(D7)

Jiang J, Tian G (2010) Analysis of the impact of land use/land cover change on land surface temperature with remote sensing. Procedia Environ Sci 2:571–575

Liu L, Zhang Y (2011) Urban heat island analysis using the Landsat TM data and ASTER data: a case study in Hong Kong. Remote Sens 3(7):1535

Kumar JAV, Pathan SK, Bhanderi RJ (2007) Spatio-temporal analysis for monitoring urban growth: a case study of Indore city. J Indian Soc Remote Sens 35:11–20

Kustas WP, Norman JM, Anderson MC, French AN (2003) Estimating subpixel surface temperatures and energy fluxes from the vegetation index-radiometric temperature relationship. Remote Sens Environ 85(4):429–440

Landis JR, Koch GG (1977) The measurement of observer agreement for categorical data. Biometrics 33:159–174

Li J, Song C, Cao L, Zhu F, Meng X, Wu J (2011) Impacts of landscape structure on surface urban heat islands: a case study of Shanghai, China. Remote Sens Environ 115:3249–3263

Li H, Liu Q, Zou J (2009) Relationships of LST to NDBI and NDVI in Changsha–Zhuzhou–Xiangtan area based on MODIS data, Scientia Geographica Sinica (Abstract only)

Liu Y, Peng J, Wang Y (2017) Diversification of land surface temperature change under urban landscape renewal: a case study in the main city of Shenzhen China. Remote Sens. 9:919

Liu F, Jia X, Li W, Du A, Wang D (2020) Analysis of land surface temperature evolution based on regional road scope. Adv Civil Eng, Hindawi

Lu D, Weng Q (2006) Use of impervious surface in urban land-use classification. Remote Environ 102(1):146–160

Lu D, Li G, Kuang W, Moran E (2013) Methods to extract impervious surface areas from satellite images. Int J Digital Earth 7(2):93–112

Mallick J, Kant Y, Bharath BD (2008) Estimation of land surface temperature over Delhi using Landsat-7 ETM+. J Ind Geophys Union 12(3):131–140

Nimish HA, Bharath AL (2020) Exploring temperature indices by deriving relationship between land surface temperature and urban landscape. Remote Sens Appl Soc Environ 18:100299

NRSC (2014) Land use/land cover database on 1:50,000 scale, Natural Resources Census Project, LUCMD, LRUMG RSAA. National Remote Sensing Centre, ISRO, Hyderabad

Owen TW, Carlson TN, Gillies RR (1998) An assessment of satellite remotely sensed land cover parameters in quantitatively describing the climatic effect of urbanization. Int J Remote Sens 19:1663–1681

Raynolds MK, Josefino CC, Donald A, Walker and Verbyla David, (2008) Relationship between satellite-derived land surface temperatures, arctic vegetation types and NDVI. Remote Sens Environ 112:1884–1894

Ridd MK (1995) Exploring a V-I-S (vegetation-impervious surface–soil) model for urban ecosystem analysis through remote sensing: comparative anatomy for cities. Int J Remote Sens 16:2165–2185

Sannigrahi S, Bhatt S, Rahmat S, Uniyal B, Banerjee S, Chakraborti S, Bhatt A (2017) Analyzing the role of biophysical compositions in minimizing urban land surface temperature and urban heating, Urban Climate, Elsevier 1–17

Sharma R, Chakraborty A, Joshi PK (2015) Geospatial quantification and analysis of environmental changes in urbanizing city of Kolkata (India). Environ Monit Assess 187(1):4206

Sheik MP (2019) Spatial-temporal variation of land surface temperature of Jubail Industrial City, Saudi Arabia due to seasonal effect by using Thermal Infrared Remote Sensor (TIRS) satellite data. J Afr Earth Sc 155:54–63

Stisen S, Sandholt I, Nørgaard A, Fensholt R, Eklundh L (2007) Estimation of diurnal air temperature using MSG SEVIRI data in West Africa. Remote Sens Environ 110(2):262–274

Sundara KK, Udaya BP, Padmakumari K (2012) Estimation of land surface temperature to study urban heat island effect using Landsat ETM_+ image. Int J Eng Sci Technol 4(02 February):771–778

Taloor AK, Manhas DS, Kothyari GC (2021) Retrieval of land surface temperature, normalized difference moisture index, normalized difference water index of the Ravi basin using Landsat data. Appl Comp Geosci 9:100051

USGS (2016) Landsat 8 (L8) Data users handbook, Department of the Interior, US Geological Survey.

Wang YC, Hu BKH, Myint SW, Feng CC, Chow WTL, Passy PF (2018) Effects of landscape composition and pattern on land surface temperature: an urban heat … patterns of land change and their potential impacts on land surface temperature change in Yangon Myanmar. Sci Total Env 643:738–750

Weng Q, Lu D, Schubring J (2004) Estimation of land surface temperature-vegetation abundance relationship for urban heat island studies. Remote Sens Environ 89:467–483

Xiao R, Weng Q, Ouyang Z, Li W, Schienke EW, Zhang Z (2008) Land surface temperature variation and major factors in Beijing China. Photogramm Eng Remote Sens 74(4th April):451–461

Xiong Y, Huang S, Chen F et al (2012) The impacts of rapid urbanization on the thermal environment: a remote sensing study of Guangzhou South China. Remote Sens 4:2033–2056

Xu H (2006) Modification of normalised difference water index (NDWI) to enhance open water features in remotely sensed imagery. Int J Remote Sens 27(14):3025–3033

Yuan F, Bauer ME (2007) Comparison of impervious surface area and normalized difference vegetation index as indicators of surface urban heat island effects in Landsat imagery. Remote Sens Environ 106(3):375–386

Zha Y, Gao J, Ni S (2003) Use of normalized difference built-up index in automatically mapping urban areas from TM imagery. Int. J. Rem. Sens. 24(3):583–594

Zhou W, Huang G, Cadenasso ML (2011) Does spatial configuration matter? Understanding the Effects of Land Cover Pattern on Land Surface Temperature in Urban Landscapes. Landsc Urban Plan 102(1):54–63